

1 High-frequency variability in the
2 North Icelandic Jet

3 B. E. Harden¹ and R. S. Pickart

4 Woods Hole Oceanographic Institution, Woods Hole, USA

5 August 2017

¹Woods Hole Oceanographic Institution, 266 Woods Hole Road, Woods Hole, MA 02543.
bharden@whoi.edu

ABSTRACT

7 We describe the high-frequency variability in the North Icelandic Jet on the Iceland Slope
8 using data from the densely instrumented Kögur mooring array deployed upstream of the
9 Denmark Strait sill from September 2011 to July 2012. Significant sub-8-day variability
10 is ubiquitous in all moorings from the Iceland slope with a dominant period of 3.6 days.
11 We attribute this variability to Topographic Rossby Waves on the Iceland slope with a
12 wavelength of 62 ± 3 km and a phase velocity of 17.3 ± 0.8 km day⁻¹ directed downslope
13 (-9°T). We test the theoretic dispersion relation for these waves against our observations
14 and find good agreement between the direction of phase propagation. We additionally
15 calculate a theoretical group velocity of 36 km day⁻¹ directed almost directly up-slope
16 (138°T) which agrees well with the propagation speed of observed energy pulses headed
17 upslope. We use a wave tracing model to show that this wave energy is generated locally,
18 offshore of the array, and not in the upstream or downstream directions. We hypothesize
19 that either the meandering Separated East Greenland Current at the foot of the Iceland
20 slope or intermittent aspiration into the Denmark Strait Overflow are the drivers of the
21 Topographic Rossby Waves. Regardless of the formation mechanism, the waves appear to
22 be a local phenomena, not found in an instrumented record upstream.

23 1. Introduction

24 The Denmark Strait Overflow is the major pathway of dense water out of the Nordic
25 Seas. It transports 3.2 Sv, or approximately 50%, of the total outflow (reference), and
26 hence plays a crucial role in the Atlantic meridional overturning circulation (AMOC).
27 While the existence of this overflow has been known for many decades, our understanding
28 of the processes that govern it and the underlying dynamics remains incomplete. One
29 important aspect that requires further study is determining the upstream sources of the
30 dense water and how it approaches the sill. If we are to determine how a changing climate
31 might impact the AMOC, we need to understand better the connection between the water
32 mass transformation process and the flux of newly ventilated water to Denmark Strait.

33 Most of the Denmark Strait Overflow water (approximately 70%) comes from the
34 East Greenland Current by way of the Nordic Seas boundary current system (Våge *et al.*,
35 2013; Harden *et al.*, 2016) (see Figure 1). Specifically, warm Atlantic inflow across the
36 Greenland-Scotland Ridge is progressively cooled as it flows northward towards Fram
37 Strait, much of it recirculating in the strait and subducting to mid-depth (Mauritzen, 1996).
38 This is joined by Atlantic water exiting the strait that has circumnavigated the Arctic, and
39 together the transformed Atlantic water flows southward in the East Greenland Current. As
40 the current rounds Scoresby Sund, it splits into two branches (Figure 1). One continues to-
41 wards the sill as a shelfbreak jet (Håvik *et al.*, 2017). The other carries approximately 60%
42 of the East Greenland Current water out into the central strait via eddies and/or gyre-like
43 deflections of the shelfbreak jet (Våge *et al.*, 2013; Harden *et al.*, 2016). This separated
44 pathway then flows into the strait along the outer Iceland slope.

45 The remaining 30% of Denmark Strait Overflow water is supplied by the North Ice-
46 landic Jet (NIJ), a more recently discovered branch of the upstream circulation (Jonsson
47 and Valdimarsson, 2004; Våge *et al.*, 2011). This mid-depth intensified jet advects waters
48 distinct from those found in the East Greenland Current (colder and fresher) suggestive of
49 a source in the central Iceland or Greenland seas (Våge *et al.*, 2011; 2015; Harden *et al.*,

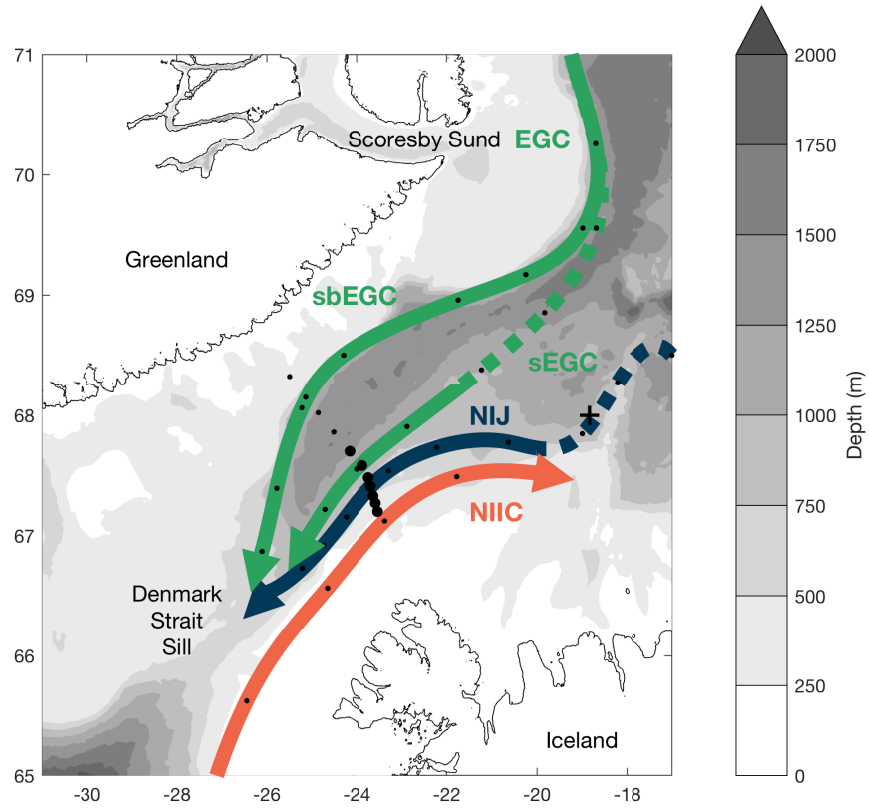


Figure 1: Map of the study region showing the overflow pathways approaching the Denmark Strait Sill: the North Icelandic Jet (NIJ) and the two East Greenland Current (EGC) pathways, one along the shelfbreak (sbEGC) and the other in a separated branch on the Iceland Slope (sEGC). Dashed portions show parts of pathways that still need further clarification. Also shown is the northward flowing surface-intensified current, the North Icelandic Irminger Current (NIIC). Block dots show the locations of the moorings in the Kögur array with larger dots indicating the subset of seven moorings used in this study. The upstream cross is the mooring to the west of the Kolbensey ridge referred to in the text. The bathymetry is from IBCAO. [WHICH VERSION OF IBCAO?]

2016). The NIJ contains the densest water that feeds the overflow; its waters are found in the deepest part of the sill (Mastropole *et al.*, 2017) and subsequently sink to the deepest depths in the core of the overflow.

The leading hypothesis for the formation of the NIJ, supported by both models and observations, is that it represents the lower limb of a local overturning cell in the Iceland sea (Våge *et al.*, 2011; Behrens *et al.*, 2017). The upper limb of the cell is the NIIC, which sheds warm water into the Iceland Sea that is cooled by air-sea heat loss. The transformed water then returns southward towards the boundary where it sinks and forms the NIJ. However, many questions remain unanswered about this proposed system. For instance, the winter mixed-layers in the Iceland Sea don't appear to be dense enough to account for the deepest water in the NIJ (Våge *et al.*, 2015), whereas those in the Greenland Sea do (Strass *et al.*, 1993; Rudels *et al.*, 2002).

Regardless of the source of the NIJ, it clearly constitutes a vital component of the circulation upstream of the sill. (Harden *et al.*, 2016) investigated the jet's mean and seasonal contribution to the overflow, demonstrating that there is time-dependent partitioning of transport between the NIJ and the other two overflow branches on weekly to monthly timescales, likely driven by the wind. Pickart *et al.* (2017-09-01T00:00:00) noted that the NIJ appears to be coupled to the northward-flowing NIIC and that, on occasion, it consists of multiple branches. Using historical hydrographic data, Pickart *et al.* (2017-09-01T00:00:00) also revealed a clear link between the interannually varying properties of the NIJ and those of the densest water at the Denmark Strait sill, leaving little doubt that the NIJ is a major source of the overflow plume.

It has long been known that the Denmark Strait Overflow varies on short (order days) timescales (Smith, 1976; Bruce, 1995; Käse *et al.*, 2003). Some of this variability is associated with the passage of lenses of cold, dense, overflow water referred to as boluses (Cooper, 1955). Recently, Appen *et al.* (2017) identified a second type of mesoscale feature in the strait that was termed a pulse. In contrast to boluses, pulses correspond to a

77 thinning of the overflow layer associated with a large increase in equatorward velocity.
78 Both of these features have been identified in a high-resolution regional model as well
79 (Almansi *et al.*, 2017). Appen *et al.* (2017) showed that, between boluses and pulses, a
80 mesoscale feature passes through Denmark Strait on average every 2 days. Presently, how-
81 ever, it is unknown if these disturbances originate from upstream or if they are associated
82 with local dynamics near the sill.

83 The goal of the present study is to describe the high frequency variability of the NIJ
84 north of the Denmark Strait and shed light as to its causes. We use timeseries data from a
85 year-long mooring array that was maintained roughly 200 km upstream of the sill (Figure
86 1). This is the same data set used by Harden *et al.* (2016) to investigate the mean and
87 seasonal attributes of the NIJ. While Harden *et al.* (2016) mentioned that the NIJ exhibits
88 high-frequency variability, they did not elaborate. We begin with a brief description of
89 the data, followed by a characterization of the high-frequency signal. We discuss how this
90 signal is consistent with the existence of Topographic Rossby waves on the Iceland slope
91 and go on to investigate the source region of the energy in these waves through inverse
92 wave tracing.

93 **2. Data and Methods**

94 The data for this study come from the densely instrumented Kögur mooring array
95 spanning the Denmark Strait approximately 200 km upstream of the sill. The array was
96 deployed for 11 months from September 2011 to July 2012 and consisted of 12 moorings
97 (named KGA 1-12) equipped with instrumentation to measure both the hydrography and
98 velocity of the water column from 50 m to the bottom. Harden *et al.* (2016) present a
99 detailed description of the mooring data, including the instrumentation, processing steps,
100 and sensor accuracies. The array captured the majority of overflow water (denser than
101 27.8 kg m^{-3}) passing through the northern part of the strait towards the sill.

102 Here we use primarily the gridded product described in Harden *et al.* (2016), which

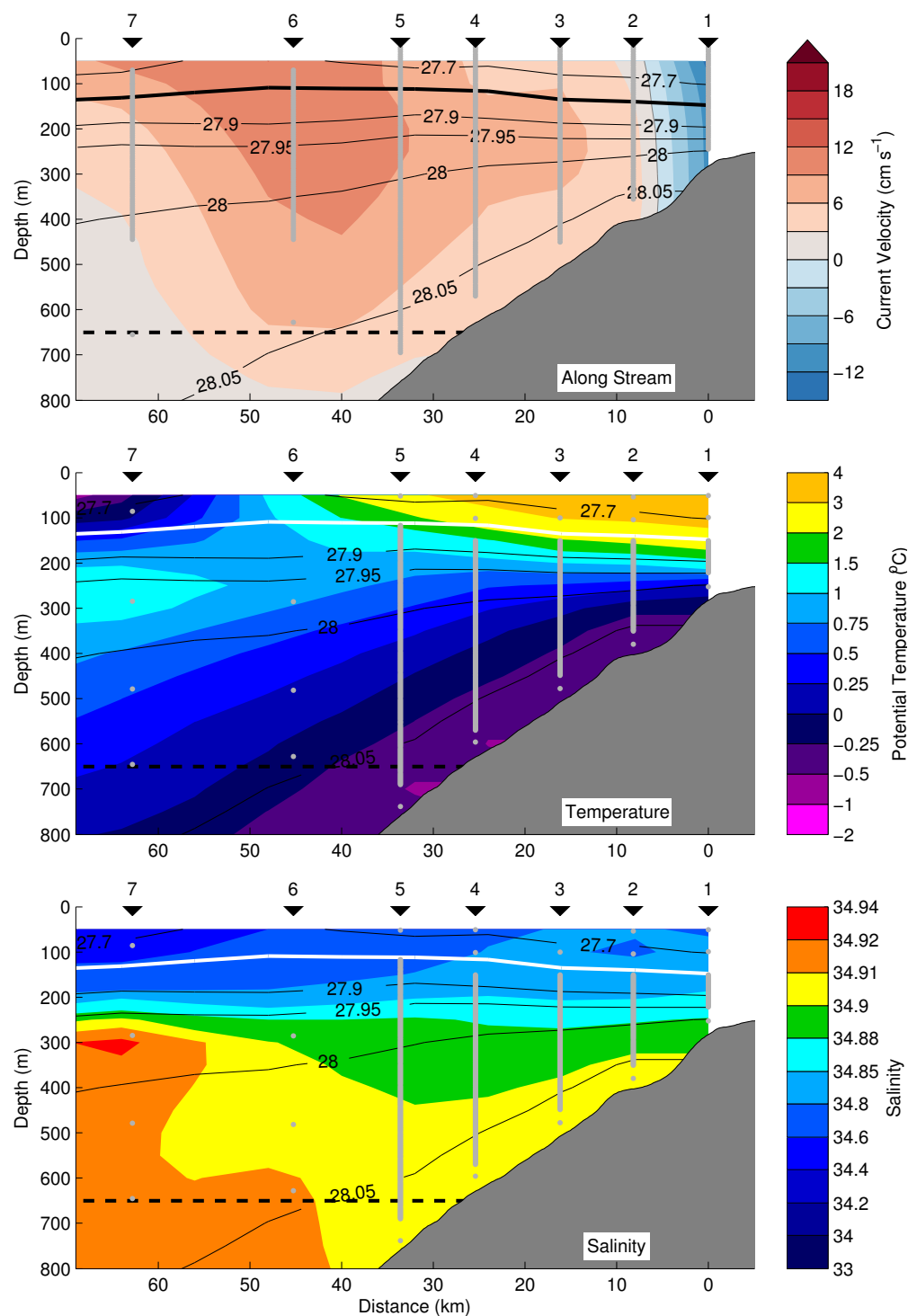


Figure 2: Mean vertical section of the along-stream (cross-transect) velocity (top), and median sections of potential temperature (middle) and salinity (bottom) for the 11-month period of the Kögur array. Overlaid in black contours on each panel is the mean density with the 27.8 kg m^{-3} isopycnal (the upper boundary of Denmark Strait Overflow Water) highlighted. The viewer is looking to the northeast with Iceland on the right. Positive velocities are equatorward. The horizontal black dashed line indicates the depth of the Denmark Strait sill. The moorings (black triangles) are labeled, and the average instrument locations are shown by the grey points. The bathymetry is from a shipboard echosounder.

103 has a lateral resolution of 8km and vertical resolution of 50 m. Because of our focus
104 on the Iceland slope, we consider a subset of these data up to and including the location
105 of mooring KGA 7, approximately 70 km offshore of the Iceland shelfbreak. The mean
106 velocity sections demonstrate that this portion of the array captures both the NIJ and the
107 majority of the Separated EGC (Figure 2). For parts of the analysis we also use the data
108 on a mooring-by-mooring basis. All of the velocities have been de-tided using a 36-hour
109 low-pass filter.

110 Additional data come from a mooring located approximately 200 km upstream of the
111 Kögur Array on the west side of the Kolbesney Ridge ($68^{\circ}00'N$, $18^{\circ}50'W$, see Figure
112 1) This was deployed on the 1000 m isobath from September 2007 to mid-October 2008
113 and consisted of a McLane moored profiler and acoustic current meter providing profiles
114 between 100 m and the bottom at 8 hour intervals. As with the Kögur data, we low-passed
115 the velocity timeseries using a 36-hr filter to remove the tidal components of the flow.
116 These data are described in greater detail by Jónsson and Valdimarsson (2012).

117 The inverse wave tracing of topographic Rossby waves (TRWs) was done using the
118 model described by Meinen *et al.* (1993) and implemented by Pickart (1995) for investigat-
119 ing TRWs in the Deep Western Boundary Current off of Cape Hatteras, North Carolina.
120 The method uses the TRW dispersion relation to calculate the group velocity and then
121 backtracks the evolution of the wave with a time step of 30 minutes. The wave parameters
122 are recalculated at each step for the local bottom depth, bottom slope, and water column
123 stratification. A new group velocity is then found and used to further trace the wave. Most
124 of the required input parameters for the inverse wave tracing model come directly from the
125 moored data and are the same as those used for the theoretical TRW dispersion relation
126 calculations (see Section 3.a.). For the bathymetry we used the International Bathymetric
127 Chart of the Arctic Ocean 30-arcsec gridded product (Jakobsson *et al.*, 2012). To remove
128 seamounts and other sharp topographic features we smoothed the bathymetry using a filter
129 of 60 km (comparable to our measured TRW wavelength). In contrast to Pickart (1995)

130 who subsequently fit splines to the data to be able to find the bottom depth and gradients
131 at any location, we deemed our resolution to be high enough (and our smoothing window
132 great enough) to simply use linear interpolation. The total integration period for the wave
133 tracing was 48 hours.

134 **3. Results**

135 As discussed in Harden *et al.* (2016), the vertical sections of velocity and hydrography
136 at the Kögur site show the signatures of both the NIJ and the Separated EGC. However, the
137 two features are merged to some degree in the mean (Figure 2). The NIJ is on the upper
138 Iceland slope and is characterized by a mid-depth intensified flow carrying the coldest,
139 densest overflow water banked up on the slope. The Separated EGC is farther offshore;
140 its key features are a surface intensification and the transport of warmer, saltier overflow
141 water at approximately 300 m. Inshore of both these currents, on the Iceland shelf, is the
142 poleward flowing NIIC (see also Figure 1).

143 The two overflow currents are merged in the mean largely due to the high degree
144 of variability on weekly timescales. The depth-integrated, along-stream velocity exhibits
145 constant pulsing through this portion of the strait (Figure 3a). The period of the pulsing
146 in the vicinity of the NIJ is concentrated at sub-8-day periods with a maximum average
147 energy at 3.6 days (Figure 4). Farther offshore, near the Separated EGC, we also see
148 such short-period pulses in addition to more consistent longer-period variability (Figure
149 3a). The lower frequency signals were described by Harden *et al.* (2016) and attributed in
150 part to the time-varying upstream bifurcation of the EGC. Here we focus on the higher-
151 frequency, sub-8-day variability. To facilitate this we used an 8-day butterworth filter.¹

152 The variance ellipses of this high-frequency variability for each mooring are useful
153 for characterizing different regimes across the array (Figure 5). In the NIIC (KGA 1), the
154 variance ellipse is elongated in the direction of the mean flow indicative of a current puls-

¹Different period filters were implemented, ranging in length from 4 days to 30 days, but the 8-day filter was most effective in isolating the peak high-frequency energy.

./figures/hoff_vars.pdf

Figure 3: Hovmöller plots from the gridded mooring data of a) the depth-mean along-stream velocity (below 100 m, same for all plots); b) the 8-day high-passed, depth-mean component of velocity in the direction major axis of the local variance ellipse; and c) the wavelet amplitude at a 4-day period for the depth-mean velocity. The wavelet analysis uses the jLab toolbox (Lilly, 2017) with standard Morlet wavelets with $\gamma=3$ and $\beta = 2$. The sloped, black guidelines are angled at the theoretical group velocity for the measured topographic Rossby waves (see text for details).

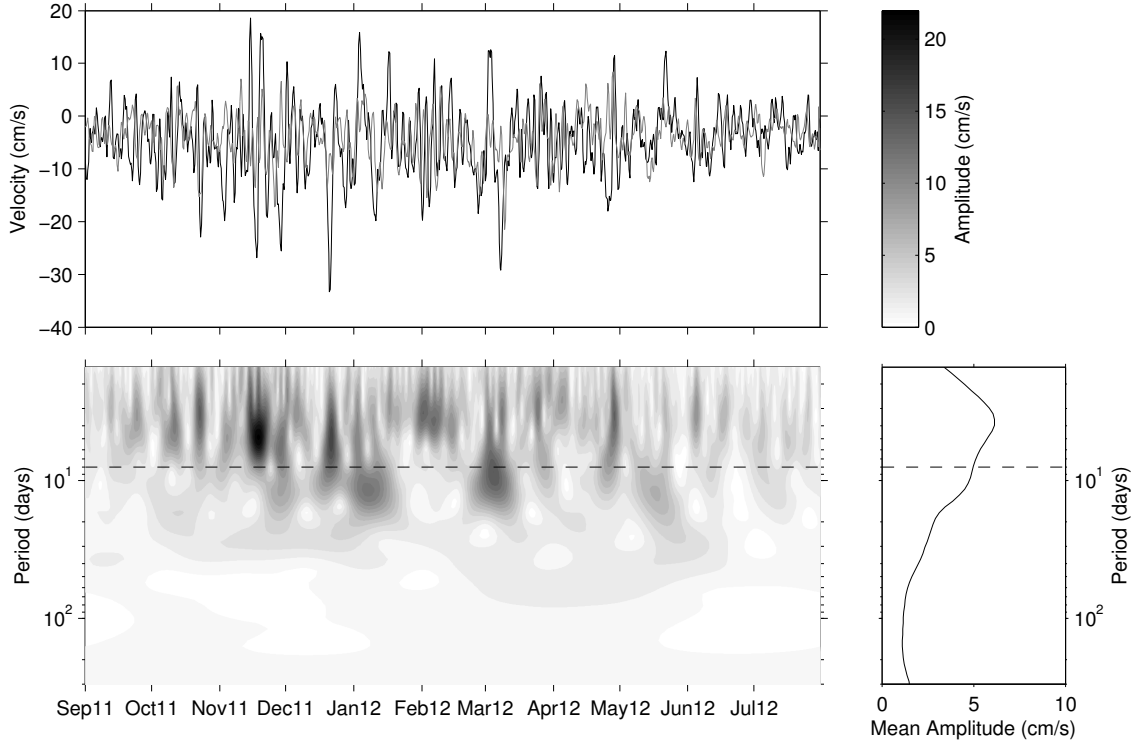


Figure 4: Top: Depth-averaged along-stream (black) and cross-stream (grey) components of velocity for the grid point closest to mooring KGA 3. Bottom left: Wavelet spectrum of the depth-averaged speed using Morlet wavelets. The color scale for this plot is at the top right. Bottom right: Mean wavelet amplitude for the length of the deployment. The dashed line in the bottom panels indicates the 8-day cut-off period for the high-pass filter.

155 ing along its axis. By contrast, within the Separated EGC (KGA 6 and 7), the elongation of
 156 the variance ellipses is perpendicular to the mean flow demonstrating that this current me-
 157 anders. However, in the NIJ (KGA 2-4), the major axes of the variance ellipses are aligned
 158 at an oblique angle to both the mean flow and the underlying bathymetry. KGA 5 appears
 159 to be in a transition region between conditions in the NIJ and those in the Separated EGC.

160 *a. Topographic Rossby Waves*

161 We resolved the sub-8-day depth-averaged flow in the gridded product along the major
 162 axis of the variance ellipses at each offshore location. Particularly in the NIJ, the variability
 163 along these axes have a sinusoidal form and are lagged between moorings such that the
 164 pulses of current progress offshore in time (Figure 3b). This implies a downslope phase

165 propagation of this variability.

166 We argue that this is the signature of TRWs. These waves are supported by topo-
 167 graphic β and result in transverse fluctuations that are often at an oblique angle to the
 168 mean flow. TRWs are found in many slope regions of the worlds oceans (Garrett, 1979;
 169 Louis *et al.*, 1982; Pickart and Watts, 1990). Key features of TRWs include wave vec-
 170 tors (and hence phase velocities) that are perpendicular to the velocity variability, a group
 171 velocity which is at an oblique angle to the phase velocity, and a tendency to be bottom-
 172 trapped in regions of significant stratification.

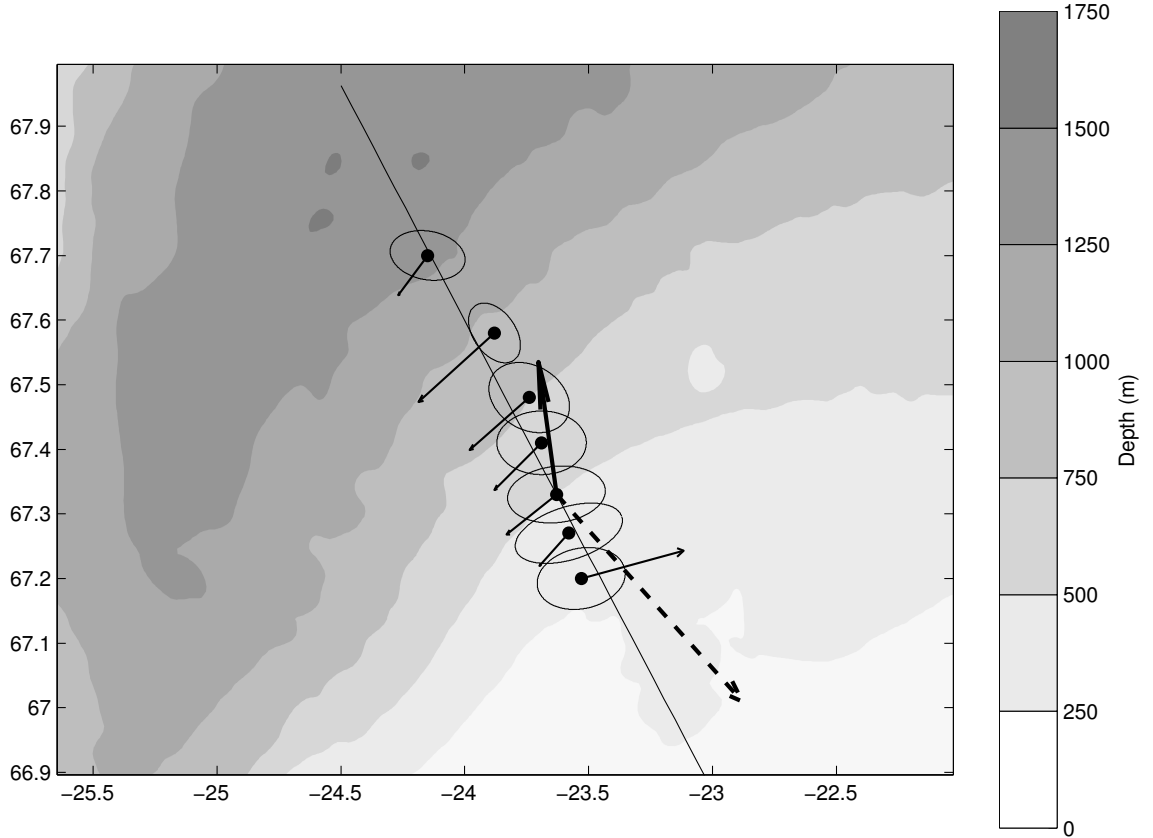


Figure 5: Aspects of the flow measured by the Kögur moorings (black circles). The thin vectors indicate the mean velocity averaged from 100 m to the depth of the ADCP at each mooring (see gray lines in Figure 2). Also shown are the 8-day high-passed variance ellipses for the same depth range. The thick black arrow denotes the direction of TRW phase propagation averaged over KGA 2-4 (plotted at KGA 3). The dashed black arrow shows the direction of TRW group velocity. The long black line is the mean downslope direction averaged between KGA 2-4. Bathymetry is from IBCAO.

173 Given that the phase propagation is perpendicular to the velocity variability, we de-
 174 duce that the wave phase is progressing downslope at -9°T (average from moorings KGA
 175 2–4, see Figure 5). Following Pickart and Watts (1990), we then calculated the phase
 176 speed over the range of moorings KGA 2–4 (where the wave signal is most pronounced)
 177 using,

$$c_p = \frac{1}{T} \frac{360}{\bar{\phi}} \frac{\overline{\Delta S}}{\cos(\Delta)}$$

178 where T is the wave period ($= 3.6$ days), $\bar{\phi}$ is the average phase offset ($= 48 \pm 3^\circ$),
 179 ΔS is the average instrument spacing ($= 8.1 \pm 0.2$ km), and Δ is the angle between the
 180 mooring array and the direction of wave propagation ($= 8 \pm 4^\circ$). The resulting phase
 181 speed is 17.3 ± 0.8 km day $^{-1}$ corresponding to a wavelength of 62 ± 3 km. The error
 182 estimates arise in equal contributions from uncertainties in $\bar{\phi}$, ΔS , and Δ .

183 As a consistency check that the observed fluctuations are in fact TRWs, we can em-
 184 ploy the TRW dispersion relation for a uniformly stratified ocean neglecting planetary β .
 185 Following Pedlosky (1979), this can be written as:

$$T = \frac{2\pi \tanh(\frac{2\pi ND}{\lambda f})}{N\Gamma \sin(\theta)}$$

186 where T is the period of the wave, N is the average water column Brunt Väisälä
 187 frequency ($= 3.3 \times 10^{-5}$, averaged using the gridded data below 100 m), D is the depth
 188 ($= 500$ m), λ is the wavelength, f is the Coriolis parameter ($= 1.35 \times 10^{-4}$), Γ is the
 189 bottom slope ($= 0.016$, from IBCAO v3), and θ is the phase velocity direction relative to
 190 downslope.

191 We can test the predicted value of θ against the observed value using our knowledge

192 of the other variables. The predicted angle of 29° compares well with the measured value
193 of 24° (from the average downslope angle between moorings KGA 2–4). There is of
194 course uncertainty in the measured downslope angle depending on the region selected
195 for the averaging. For example, if we expand the calculation of the downslope direction
196 to encompass KGA 1–5, the measured θ becomes 33° , which still agrees well with the
197 predicted value. In addition, the bottom-trapping scale ($=f/Nk$) is much greater than
198 1000 m, in agreement with the observed velocities which are largely barotropic.

199 All of this supports our assertion that the dominant high-frequency variability in the
200 NIJ is due to TRWs. The obvious question is, where and how are these waves being
201 generated? Using the dispersion relation we can calculate the group velocity. For the
202 observed parameters, we find this to be 36 km day^{-1} directed almost directly up-slope at
203 the array site (138°T , see Figure 5). This implies that the energy source lies offshore.
204 We can corroborate this onshore propagation of energy observationally by considering the
205 wavelet amplitude for the 4-day signal at each mooring site. The Hovmöller plot of this
206 shows clear occurrences of onshore energy propagation that are in line with the predicted
207 group velocity (Figure 3c).

208 *b. Wave Tracing and TRW Formation Mechanisms*

209 In order to shed light on the source of the TRWs, we implemented the inverse wave
210 tracing model described in Section 2. In particular, we calculated the wave paths back-
211 wards in time from moorings KGA 2–5. For each mooring, the model was initialized
212 with the local wavenumber (assuming constant phase velocity and wave period). Since
213 KGA 5 only marginally displayed TRW behavior, the results from that mooring should
214 be considered less robust. The calculated paths indicate that the waves originate offshore
215 of the moorings in the vicinity of the deep Blosseville Basin (Figure 6). While the traces
216 diverge somewhat going offshore, it is clear that they do not deflect significantly upstream
217 or downstream. In other words, the energy is not propagating along the Iceland continental
218 slope.

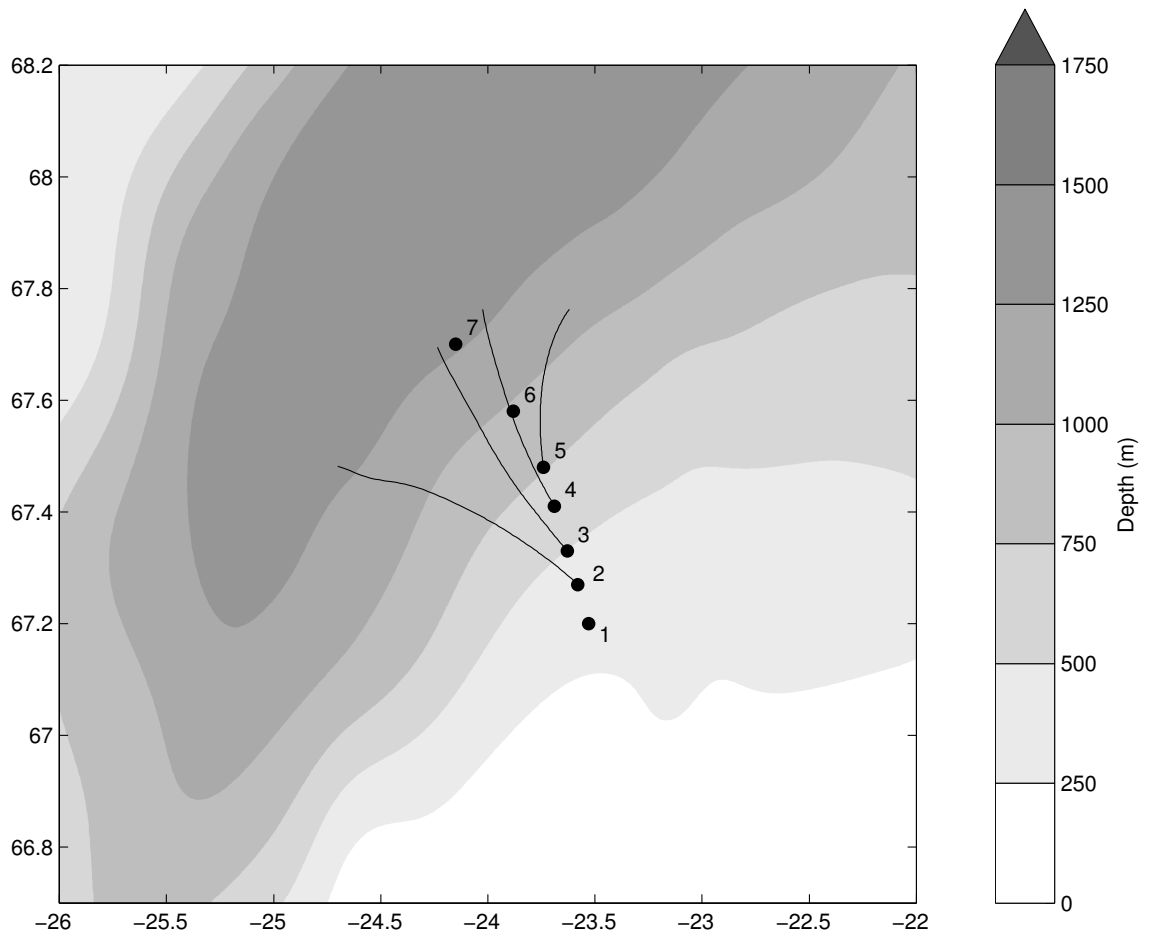


Figure 6: Paths of the topographic Rossby waves (thin lines) computed using the inverse wave tracing model for moorings KGA 2-5. The bathymetry is from IBCAO v3 smoothed over 60 km (see text for details).

219 TRWs are a ubiquitous feature in the middle Atlantic Bight between Cape Hatteras,
220 NC and the Grand Banks (Louis *et al.*, 1982; Johns and Watts, 1986; Pickart and Watts,
221 1990). The source of the waves appears to be the Gulf Stream. Both Hogg (1981) and
222 Schultz (1987) argued that TRWs observed along the US continental slope emanated from
223 large amplitude Gulf Stream meanders offshore. Louis *et al.* (1982) made the case that
224 bursts of TRWs measured south of Nova Scotia resulted from Gulf Stream eddy formation.
225 Pickart (1995) demonstrated that the TRWs observed near Cape Hatteras were forced by
226 meanders of the Gulf Stream as it flowed over a bend in topography farther to the east.

227 In light of these studies, it is natural to suspect that the TRWs measured at the Kögur
228 array site are generated by the Separated EGC. This current is energetic, and, as noted
229 above, is subject to significant meandering (akin to the Gulf Stream). The wave tracing
230 indicates that the energy emanates from the Blosseville Basin where the Separated EGC
231 resides. Additionally, there is evidence that times of strong TRW activity on the upper
232 slope are often preceded slightly by increases in meander energy offshore (Figure 3). The
233 high-energy event in November is one example of this, but there are additional instances
234 in late October, late December, and early March.

235 Another possible trigger for the waves is the intermittent aspiration of deeper waters
236 towards the Denmark Strait Sill. Harden *et al.* (2016) demonstrated that 0.6 Sv of the
237 overflow transport approaching the sill does so from below sill depth. Pulsing of this
238 aspirated component of the flow across the isobaths could initiate topographic wave activ-
239 ity. Regardless of the mechanism, the presence of TRWs raises the question of whether
240 they are present along the entire Iceland slope or whether they are unique to our sampling
241 region. To address this we examined the velocity data from a mooring deployed approxi-
242 mately 200 km upstream on the Iceland slope near the Kolbeinsey ridge from 2007–2008
243 (Jónsson and Valdimarsson, 2012). The depth-mean velocity showed very little energy
244 in the 4-day period, at odds with the large TRW signal found at this period at the Kögur
245 array. Notably, the upstream mooring site is quite far from the Separated EGC (Figure 1)

246 and hence lacks that as an energy source.

247 **4. Summary and Discussion**

248 We have documented the existence of energetic Topographic Rossby Waves (TRWs)
249 within the North Icelandic Jet (NIJ) using observations from the densely-instrumented
250 Kögur Array located approximately 200 km upstream of the Denmark Strait Sill. The
251 mean period of the waves is 3.6 days, the wavelength is 64 ± 3 km, and the phase velocity
252 is 17.7 ± 0.8 km day⁻¹ directed downslope (-9°T). Using the TRW dispersion relation,
253 we corroborated our observed direction of phase propagation relative to the downslope
254 direction (25°) with the theoretical value (26°). We further calculated that the wave energy
255 is progressing up-slope (137°T) at 39 km day⁻¹, in agreement with our observational
256 data. It is likely that the energy in the TRWs emanates locally near the mooring site,
257 either through the meandering of the offshore Separated East Greenland Current (EGC),
258 or through pulses of cross-bathymetric flow due to the aspiration of deep overflow water
259 as it approaches Denmark Strait.

260 Notably, our data imply that the dominant high-frequency variability at the Kögur site
261 does not originate from the Denmark Strait, nor does it propagate towards the sill. This
262 is perhaps surprising in light of the fact that fluctuations of the dense overflow water at
263 the sill occur on similar short timescales (Jochumsen *et al.*, 2017). It suggests that the
264 mesoscale features (boluses and pulses) diagnosed observationally by Appen *et al.* (2017)
265 and in a model framework by Almansi *et al.* (2017) are generated locally in the vicinity
266 of the sill. On the other hand, the Denmark Strait overflow is believed to be subject to
267 hydraulic control (Whitehead, 1998; Nikolopoulos *et al.*, 2003). Consequently, when there
268 are variations at the sill the information should be transferred upstream towards the Iceland
269 Sea, likely as Kelvin waves. Our results indicate that any such signals are dominated by
270 the locally-generated TRW energy. However, this deserves more careful investigation,
271 and the question of how signals are transferred between the sill and the Iceland slope is

272 the subject of an on-going study.

273 Finally, one also needs to consider where the energy in the TRWs ends up and what
274 impact it has on the dynamics of the circulation inshore of the Iceland slope. One possi-
275 bility is that the energy cascades into the North Icelandic Irminger Current (NIIC) where
276 it dissipates, leading to enhanced mixing. It might also alter the stability of NIIC, which
277 brings warm subtropical water into the Nordic Seas. (Våge *et al.*, 2011) hypothesize that
278 the offshore flux of this warm water associated with the disintegration of the NIIC is tied
279 to the overturning loop that forms the NIJ. Notably, eddies of NIIC water are found both
280 in the Blosseville Basin (Jónsson and Valdimarsson, 2012) and farther north in the Iceland
281 Sea (Våge *et al.*, 2011). It is intriguing to think that the TRWs described here could play
282 a role in this aspect of the NIIC.

283 *Acknowledgments.* We would like to thank the crew and technicians aboard the R/V
284 Knorr and RSS James Clark Ross for the deployment and recovery of the Kögur moorings.
285 This work was supported by National Science Foundation grants OCE-0959381 (BH and
286 RP) and OCE-1558742 (RP).

287

288 REFERENCES

- 289 Almansi, M., T. W. N. Haine, R. S. Pickart, M. G. Magaldi, R. Gelderloos, and D. Mas-
290 tropole. 2018/01/05 2017. High-frequency variability in the circulation and hydrog-
291 raphy of the denmark strait overflow from a high-resolution numerical model. *Journal*
292 *of Physical Oceanography*, 47(12), 2999–3013. doi: 10.1175/JPO-D-17-0129.1. URL
293 <https://doi.org/10.1175/JPO-D-17-0129.1>.
- 294 Appen, W.-J. v., D. Mastropole, R. S. Pickart, H. Valdimarsson, S. Jónsson, and J. B.
295 Girton. 2017/08/03 2017. On the nature of the mesoscale variability in denmark strait.

Journal of Physical Oceanography, 47(3), 567–582. doi: 10.1175/JPO-D-16-0127.1.
 URL <https://doi.org/10.1175/JPO-D-16-0127.1>.

Behrens, E., K. Våge, B. Harden, A. Biastoch, and C. W. Böning. 2017. Composition and variability of the denmark strait overflow water in a high-resolution numerical model hindcast simulation. Journal of Geophysical Research: Oceans, 122(4), 2830–2846. doi: 10.1002/2016JC012158. URL <http://dx.doi.org/10.1002/2016JC012158>.

Bruce, J. 1995. Eddies southwest of the Denmark Strait. Deep Sea Research Part I: Oceanographic Research Papers, 42(1), 13–29. doi: 10.1016/0967-0637(94)00040-Y. URL <http://www.ingentaconnect.com/content/els/09670637/1995/00000042/000>

Cooper, L. H. N. 1955. Deep water movements in the north atlantic as a link between climatic changes around iceland and biological productivity of the english channel and celtic sea. Journal of Marine Research, pages 347–362.

Garrett, C. 2017/08/08 1979. Topographic rossby waves off east australia: Identification and role in shelf circulation. Journal of Physical Oceanography, 9(2), 244–253. doi: 10.1175/1520-0485(1979)009<0244:TRW0EA>2.0.CO;2. URL [https://doi.org/10.1175/1520-0485\(1979\)009<0244:TRW0EA>2.0.CO;2](https://doi.org/10.1175/1520-0485(1979)009<0244:TRW0EA>2.0.CO;2).

Harden, B. E., R. S. Pickart, H. Valdimarsson, K. Våge, L. de Steur, C. Richards, F. Bahr, D. Torres, E. Børve, S. Jónsson, A. Macrander, S. Østerhus, L. Håvik, and T. Hattermann. 6 2016. Upstream sources of the denmark strait overflow: Observations from a high-resolution mooring array. Deep Sea Research Part I: Oceanographic Research Papers, 112, 94–112. doi: <https://doi.org/10.1016/j.dsr.2016.02.007>. URL <http://www.sciencedirect.com/science/article/pii/S0967063715301266>.

Håvik, L., K. Våge, R. S. Pickart, B. Harden, W. J. von Appen, S. Jónsson, and S. Øster-

hus. 2017/08/30 2017. Structure and variability of the shelfbreak east greenland current
north of denmark strait. *Journal of Physical Oceanography*. doi: 10.1175/JPO-D-17-
0062.1. URL <https://doi.org/10.1175/JPO-D-17-0062.1>.

Hogg, N. G. 1981. Topographic waves along 70°w on the continental rise. *Journal of*
Marine Research, 39, 627–649.

Jakobsson, M., L. Mayer, B. Coakley, J. A. Dowdeswell, S. Forbes, B. Fridman, H. Hod-
nesdal, R. Noormets, R. Pedersen, M. Rebesco, H. W. Schenke, Y. Zarayskaya, D. Ac-
cettella, A. Armstrong, R. M. Anderson, P. Bienhoff, A. Camerlenghi, I. Church,
M. Edwards, J. V. Gardner, J. K. Hall, B. Hell, O. Hestvik, Y. Kristoffersen, C. Mar-
cussen, R. Mohammad, D. Mosher, S. V. Nghiem, M. T. Pedrosa, P. G. Travaglini, and
P. Weatherall. 2012. The international bathymetric chart of the arctic ocean (ibcao) ver-
sion 3.0. *Geophysical Research Letters*, 39(12), n/a–n/a. doi: 10.1029/2012GL052219.
URL <http://dx.doi.org/10.1029/2012GL052219>.

Jochumsen, K., M. Moritz, N. Nunes, D. Quadfasel, K. M. H. Larsen,
B. Hansen, H. Valdimarsson, and S. Jonsson. 2017. Revised trans-
port estimates of the denmark strait overflow. *Journal of Geophysical Re-*
search: Oceans, 122(4), 3434–3450. doi: 10.1002/2017JC012803. URL
<http://dx.doi.org/10.1002/2017JC012803>.

Johns, W. E. and D. R. Watts. 1986. Time scales and structure of topo-
graphic rossby waves and meanders in the deep gulf stream. *Journal of Ma-*
rine Research, 44(2), 267–290. doi: 10.1357/002224086788405356. URL
<http://www.ingentaconnect.com/content/jmr/jmr/1986/00000044/00000002>

Jonsson, S. and H. Valdimarsson. February 2004. A new path for the denmark strait over-
flow water from the iceland sea to denmark strait. *Geophys. Res. Lett.*, 31(3), L03305–.
ISSN 0094-8276. URL <http://dx.doi.org/10.1029/2003GL019214>.

- 346 Jónsson, S. and H. Valdimarsson. 06 2012. Hydrography and circulation over the southern
347 part of the Kolbeinsey Ridge. *ICES Journal of Marine Science: Journal du Conseil*.
- 348 Käse, R. H., J. B. Girton, and T. B. Sanford. 2003. Structure and variability
349 of the Denmark Strait Overflow: Model and observations. *Journal of Geophysical Research: Oceans*, 108(C6), 3181. doi: 10.1029/2002JC001548. URL
350 <http://dx.doi.org/10.1029/2002JC001548>.
351
- 352 Lilly, J. M. 2017. jlab: A data analysis package for matlab, v 1.6.3.
- 353 Louis, J. P., B. D. Petrie, and P. C. Smith. 2017/08/08 1982. Observations
354 of topographic rossby waves on the continental margin
355 off nova scotia. *Journal of Physical Oceanography*, 12(1), 47–55.
356 doi: 10.1175/1520-0485(1982)012<0047:OOTRWO>2.0.CO;2. URL
357 [https://doi.org/10.1175/1520-0485\(1982\)012<0047:OOTRWO>2.0.CO;2](https://doi.org/10.1175/1520-0485(1982)012<0047:OOTRWO>2.0.CO;2).
- 358 Mastropole, D., R. S. Pickart, H. Valdimarsson, K. Våge, K. Jochumsen, and J. Girton.
359 2017. On the hydrography of denmark strait. *Journal of Geophysical Research: Oceans*, 122(1), 306–321. doi: 10.1002/2016JC012007. URL
360 <http://dx.doi.org/10.1002/2016JC012007>.
361
- 362 Mauritzen, C. 1996. Production of dense overflow waters feeding the North
363 Atlantic across the Greenland-Scotland Ridge. Part 1: Evidence for a revised
364 circulation scheme. *Deep Sea Research Part I: Oceanographic Research Papers*, 43(6), 769–806. doi: 10.1016/0967-0637(96)00037-4. URL
365 <http://www.sciencedirect.com/science/article/pii/0967063796000374>.
366
- 367 Meinen, C., E. Fields, R. S. Pickart, and D. R. Watts. 1993. Ray tracing on topographic
368 rossby waves. Technical Report 93-1, University of Rhode Island.
- 369 Nikolopoulos, A., K. Borenäs, R. Hietala, and P. Lundberg. 2003. Hydraulic
370 estimates of Denmark Strait overflow. *Journal of Geophysical Research*.

371 search: Oceans, 108(C3), 3095. doi: 10.1029/2001JC001283. URL
 372 <http://dx.doi.org/10.1029/2001JC001283>.

373 Pedlosky, J. 1979. *Geophysical Fluid Dynamics*. Springer US. doi: 10.1007/978-1-4684-
 374 0071-7.

375 Pickart, R. S. 1995. Gulf stream-generated topographic rossby
 376 waves. Journal of Physical Oceanography, 25(4), 574–586.
 377 doi: 10.1175/1520-0485(1995)025<0574:GSTRW>2.0.CO;2. URL
 378 [https://doi.org/10.1175/1520-0485\(1995\)025<0574:GSTRW>2.0.CO;2](https://doi.org/10.1175/1520-0485(1995)025<0574:GSTRW>2.0.CO;2).

379 Pickart, R. S. and D. R. Watts. 1990. Deep western boundary current vari-
 380 ability at cape hatteras. Journal of Marine Research, 48(4), 765–791. URL
 381 <http://www.ingentaconnect.com/content/jmr/jmr/1990/00000048/00000004>

382 Pickart, R. S., M. A. Spall, D. J. Torres, K. Våge, H. Valdimarsson,
 383 C. Nobre, G. W. K. Moore, S. Jonsson, and D. Mastropole. 2017-09-
 384 01T00:00:00. The north icelandic jet and its relationship to the north ice-
 385 landic irmingier current. Journal of Marine Research, 75(5), 605–639. URL
 386 <http://www.ingentaconnect.com/content/jmr/jmr/2017/00000075/00000005>

387 Rudels, B., E. Fahrbach, J. Meincke, G. Budéus, and P. Eriksson. 2002. The East Green-
 388 land Current and its contribution to the Denmark Strait overflow. ICES Journal of Ma-
 389 rine Science: Journal du Conseil, 59, 1133–1154. doi: 10.1006/jmsc.2002.1284.

390 Schultz, R. J., 1987. Structure and propagation of topographic rossby waves northeast of
 391 cape hatteras, north carolina. Master’s thesis, Marine Science Program, University of
 392 North Carolina.

393 Smith, P. C. May 1976. Baroclinic Instability in the Denmark
 394 Strait Overflow. J. Phys. Oceanogr., 6(3), 355–371. ISSN 0022-

3670. doi: 10.1175/1520-0485(1976)006<0355:BIITDS>2.0.CO;2. URL
[http://dx.doi.org/10.1175/1520-0485\(1976\)006<0355:BIITDS>2.0.CO;2](http://dx.doi.org/10.1175/1520-0485(1976)006<0355:BIITDS>2.0.CO;2).

Strass, V. H., E. Fahrbach, U. Schauer, and L. Sellmann. 1993. Formation of Denmark Strait overflow water by mixing in the East Greenland Current. *Journal of Geophysical Research: Oceans*, 98(C4), 6907–6919. doi: 10.1029/92JC02732. URL
<http://dx.doi.org/10.1029/92JC02732>.

Våge, K., R. S. Pickart, M. A. Spall, H. Valdimarsson, S. Jónsson, D. J. Torres, S. Østerhus, and T. Eldevik. 2011. Significant role of the North Icelandic Jet in the formation of Denmark Strait overflow water. *Nature Geosci*, 4(10), 723–727. ISSN 1752-0894. doi: 10.1038/ngeo1234. URL <http://dx.doi.org/10.1038/ngeo1234>.

Våge, K., R. S. Pickart, M. A. Spall, G. W. K. Moore, H. Valdimarsson, D. J. Torres, S. Y. Erofeeva, and J. E. Ø. Nilsen. 2013. Revised circulation scheme north of the Denmark Strait. *Deep Sea Research Part I: Oceanographic Research Papers*, 79(0), 20–39. doi: 10.1016/j.dsr.2013.05.007. URL
<http://www.sciencedirect.com/science/article/pii/S0967063713001040>.

Våge, K., G. W. K. Moore, S. Jónsson, and H. Valdimarsson. 2015. Water mass transformation in the Iceland Sea. *Deep Sea Research Part I: Oceanographic Research Papers*, 101(0), 98–109. doi: 10.1016/j.dsr.2015.04.001. URL
<http://www.sciencedirect.com/science/article/pii/S0967063715000680>.

Whitehead, J. A. 1998. Topographic control of oceanic flows in deep passages and straits. *Reviews of Geophysics*, 36(3), 423–440. doi: 10.1029/98RG01014. URL
<http://dx.doi.org/10.1029/98RG01014>.